Atmos. Chem. Phys. Discuss., 11, 597–625, 2011
www.atmos-chem-phys-discuss.net/11/597/2011/
doi:10.5194/acpd-11-597-2011

Atmospheric Chemistry and Physics Discussions

An analysis of cloud overlap at a midlatitude atmospheric observation facility

L. Oreopoulos[1] **and P. M. Norris**[2,3]

[1]Laboratory for Atmospheres, NASA-GSFC, Greenbelt, MD, USA
[2]Global Modeling and Assimilation Office, NASA-GSFC, Greenbelt, MD, USA
[3]GEST, University of Maryland Baltimore County, Baltimore, MD, USA

Received: 7 December 2010 – Accepted: 11 December 2010 – Published: 7 January 2011

Correspondence to: L. Oreopoulos (lazaros.oreopoulos@nasa.gov)

Published by Copernicus Publications on behalf of the European Geosciences Union.

Abstract

An analysis of cloud overlap based on high temporal and vertical resolution retrievals of cloud condensate from a suite of ground instruments is performed at a mid-latitude observational facility. Two facets of overlap are investigated: cloud fraction overlap, expressed in terms of a parameter "alpha" indicating the relative contributions of maximum and random overlap, and overlap of horizontal distributions of condendsate, expressed in terms of the correlation coefficient of condensate ranks. The degree of proximity to the random and maximum overlap assumptions is also expressed in terms of a decorrelation length, a convenient scalar parameter that emerges under the assumption that overlap parameters decay exponentially with separation distance. Both cloud fraction overlap and condensate overlap show significant seasonal variations with a clear tendency for overlap to be closer to maximum for summer months. A tendency for more maximum overlap is also observed as the size of the domain used to define cloud fractions increases. These dependencies are significantly weaker for rank correlations. Hitherto unexplored overlap parameter dependencies are investigated by analyzing mean parameter value differences at fixed separation distance within different layers of the atmospheric column, and by searching for possible systematic relationships between alpha and rank correlation. We find that for the same separation distance the overlap parameters are significantly distinct in different atmospheric layers, and that a tendency exists for random cloud fraction overlap to be generally in sync with more random overlap of condensate ranks.

1 Introduction

While conspicuous, cloud heterogeneity is generally ignored in atmospheric research applications. The underlying reasons for doing so include computational expediency, inability to diagnose or predict the heterogeneity, and insufficient understanding of how to meaningfully convey its impact on various atmospheric processes. For example, while radiative transfer can in principle be accurately performed on a fully described 3-D cloud field, this capability cannot be trivially extended to Global Climate Models (GCMs). Obstacles like the unavailability of such finite edge 3-D cloud fields, the lack of knowledge on how to make the resulting 3-D radiation fields relevant for other model processes, and computational costs are not easy to overcome. Nevertheless, while recreating full-blown 3-D cloud heterogeneity appears to be presently out of reach in GCMs, the representation of in-cloud horizontal and vertical variability of condensate in otherwise plane-parallel clouds, seems like a tenable goal with present modeling and observational capabilities.

Recently, the coupling of cloud generators producing horizontal and vertical cloud variability with standard GCM radiative transfer algorithms operating stochastically (to maintain acceptable computational cost) has been suggested as a way to bypass direct incorporation of complex cloud structure in radiation schemes (Pincus et al., 2003). Cloud generators can also be used for pairing GCM cloud fields with simulators of instruments of much higher spatial resolution than the model grid size. But for cloud generators to produce realistic one-point statistics of cloud condensate, and therefore radiation fields, both the horizontal variability and vertical correlations of cloud fraction and condensate distributions need to be realistically described.

In this paper we provide a detailed examination of cloud vertical variability as inferred by a dataset of 2-D distributions of condensate derived from a suite of surface-based instruments. Our immediate goal is to understand the features, dependencies, and intrinsic connections between two aspects of cloud vertical variability, cloud fraction overlap and overlap of the horizontal distributions of cloud condensate. The ultimate objective, once studies such as this are carried out for a more extensive range of cloud regimes, is to determine a simple but robust set of global rules that can be used to generate modeled clouds that resemble (in terms of one-point statistics) the original cloud fields and produce similar radiative fluxes and heating rates. While measurements similar to those used here have been previously analyzed in studies of cloud fraction overlap (from ground or space), condensate distribution overlap and its relationship with cloud fraction overlap has not been studied before with an observationally-based dataset.

2 Dataset, definitions, and overlap metrics

Our overlap analysis relies solely on the continuous baseline microphysical retrieval MICROBASE evaluation product (Miller et al., 2003) of the Atmospheric Radiation Measurement (ARM) Climate Research Facility (ACRF), now part of the US Department of Energy Atmospheric System Research (ASR) Program. The MICROBASE retrieval algorithm uses a combination of observations from a millimeter cloud radar (MMCR), a ceilometer, a micropulse lidar (MPL), a microwave radiometer (MWR), and balloon-borne soundings to determine the profiles of liquid/ice water content (LWC/IWC), liquid/ice cloud particle effective radius, and cloud fraction. For liquid cloud layers (atmospheric temperatures greater than 273 K) MICROBASE uses the radar reflectivity-LWC relationship derived by Liao and Sassen (1994). The LWC profile is vertically integrated to provide a liquid water path (LWP) which is then linearly scaled to match the LWP observed by the MWR. For atmospheric temperatures below 257 K all water is assumed to be in the ice phase, and its content is determined using the radar reflectivity-IWC relationship of Liu and Illingworth (2000). Between 257 and 273 K water is assumed to exist in both phases and a linear temperature-dependent partition of ice/liquid is applied. The radar reflectivities used in the above relationships come from the Active Remote Sensing of Clouds (ARSCL) product (Clothiaux et al., 2000). While particle size retrievals are also performed as part of the MICROBASE algorithm, they are not used in the present study. Cells that are flagged to have no reflectivity data are discarded and not used in the analysis.

The MICROBASE data of this study are for the Southern Great Plains (SGP) ACRF site in Oklahoma, USA (http://www.arm.gov/sites/sgp). The dataset spans seven years (2000–2006) and data availability, although not uniform, covers all 84 months. The 2-D condensate distribution is available at a 10 s resolution along the advection path

ACPD
11, 597–625, 2011

L. Oreopoulos and P. M. Norris

of the clouds over the instruments, and 45 m vertical resolution (constrained by the MMCR range gate). For the purposes of this study, the condensate profiles for each day are divided into segments that roughly correspond to scales of typical GCMs. For example, when six segments are used per day, each segment consists in general of 1440 condensate profiles, which correspond to scales of ∼150 km assuming typical wind speeds of 10 m/s. These 1440-profile segments are our default choice for the overlap analysis, with 720- and 2880-profile segments used only when we want to highlight the sensitivity of an overlap metric to the pseudo-spatial reference scale.

Our analysis does not distinguish between the liquid and ice phases, but rather operates on the total water content, i.e., the sum of LWC and IWC. For our cloud fraction overlap analysis we calculate the true combined segment cloud fraction $C_t(z_1, z_2)$ of a pair of layers separated by distance $\Delta z = z_2 - z_1$ – where z_2 and z_1 are the heights of the layer centers as determined by the vertical resolution of the dataset, so that Δz is always a multiple of 45 m – by counting the number of profiles which have non-zero total water content at either or both of the two height levels of interest and dividing by the total number of profiles with valid cells at both heights. Individual layer cloud fractions $C(z_1)$ and $C(z_2)$ are calculated by dividing the number of cloudy (total water content greater than zero) cells in each layer by the same number of valid profiles as in the calculation of $C_t(z_1, z_2)$. From the individual layer cloud fractions, combined cloud fractions corresponding to the maximum and random overlap assumption can be calculated as follows:

$$C_{\mathrm{max}}(z_1, z_2) = \max(C(z_1), C(z_2)) \tag{1a}$$

$$C_{\mathrm{ran}}(z_1, z_2) = 1 - (1 - C(z_1))(1 - C(z_2)) \tag{1b}$$

Hogan and Illingworth (2000) proposed that the combined cloud fraction of two layers can be approximated as a weighted average of $C_{\mathrm{max}}(z_1, z_2)$ and $C_{\mathrm{ran}}(z_1, z_2)$ according to:

$$C(z_1, z_2) = \alpha(z_1, z_2) C_{\mathrm{max}}(z_1, z_2) + (1 - \alpha(z_1, z_2)) C_{\mathrm{ran}}(z_1, z_2) \tag{2}$$

ACPD
11, 597–625, 2011

An analysis of cloud overlap

L. Oreopoulos and P. M. Norris

When $C_t(z_1,z_2)$ is known, as in our case, it can be substituted in the left hand side of the above equation which can then be solved for the weighting parameter $\alpha(z_1,z_2)$, a measure of the proximity of overlap to maximum (exact when $\alpha(z_1,z_2)$=1) or random (exact when $\alpha(z_1,z_2)$=0). Negative values suggest some degree of minimum overlap (a combined cloud fraction greater than that of random overlap). Without distinguishing between contiguous and non-contiguous cloud layers, we calculate $\alpha(z_1,z_2)$ for our entire dataset for each possible cloud fraction pair for separation distances ranging from 45 to 12 015 m (1 to 267 layer separations) as long as as neither of the cloud fractions is zero or one. This procedure results in a very large dataset of $\alpha(z_1,z_2)$ values which we segregate by month. The number of valid $\alpha(z_1,z_2)$ values within a month over 7 years can exceed 7 million for 150 km segments. In the following we frequently refer to this parameter simply as "alpha".

In a similar fashion, we calculate rank correlations of total water content as a function of separation distance (see also Pincus et al., 2005). For layers at heights z_1 and z_2, the overlapping cloudy cells are identified (i.e., non-zero total water contents in both layers), and their water contents are ranked at each height. A linear correlation coefficient $r(z_1,z_2)$ is then calculated from the ranks $R_i(z_1)$ and $R_i(z_2)$ according to:

$$r(z_1,z_2) = \frac{\sum_{i=1}^{N_{\mathrm{cld}}} \left(R_i(z_1) - \overline{R}(z_1)\right)\left(R_i(z_2) - \overline{R}(z_2)\right)}{\sqrt{\sum_{i=1}^{N_{\mathrm{cld}}} \left(R_i(z_1) - \overline{R}(z_1)\right)^2}\sqrt{\sum_{i=1}^{N_{\mathrm{cld}}} \left(R_i(z_2) - \overline{R}(z_2)\right)^2}} \quad (3)$$

where N_{cld} is the number of overlapping cells and $\overline{R}(z_1)$, $\overline{R}(z_2)$ are the mean ranks of the water contents in the two layers. Unlike $\alpha(z_1,z_2)$ calculations, overcast layers are not excluded. It should also be pointed out that since the overlapping portion changes continuously with the pairing partner, the part of a specific layer being ranked is in general different for each rank correlation calculation. In other words, ranks are calculated anew as dictated by the common portion of the two layers. The rank correlation

ACPD
11, 597–625, 2011

coefficient expresses the likelihood that water contents of the same relative strength within their respective layers are aligned in the vertical, with $r(z_1,z_2)=1$ corresponding to perfect alignment and $r(z_1,z_2)=0$ corresponding to perfectly random alignment. The manner in which water contents align in the vertical is important for processes like radiation. For example, the domain-averaged fluxes differ between a case where all high or low condensate values are aligned to create pockets of vertically integrated high or low liquid water paths and a case where a more random alignment homogeneizes the horizontal distribution of LWP (e.g., see Norris et al., 2008). The full dataset of all possible $r(z_1,z_2)$ values is derived from MICROBASE condensate for the period 2000–2006 in a manner similar to alpha, described above, including segregation by month.

It has been suggested (e.g., Hogan and Illingworth, 2000; Pincus et al., 2005; Shonk et al., 2010) that profiles of alpha and rank correlation can be modeled as inverse exponential functions

$$\alpha(\bar{h},\Delta z)=\exp\left(-\frac{\Delta z}{L_\alpha(\bar{h})}\right) \tag{4a}$$

$$r(\bar{h},\Delta z)=\exp\left(-\frac{\Delta z}{L_\mathrm{r}(\bar{h})}\right) \tag{4b}$$

where L_α and L_r are decorrelation length scales which can be viewed as alternate measures of the degree of overlap. Specifically, large values of L_α indicate proximity to maximum overlap, while small values proximity to random overlap. Likewise, large values of L_r indicate condensate values that are highly correlated in terms of relative strength while small values suggest condensate values whose relative strength exhibits weak correlation between layers. In Eq. (4) the overlap parameters and decorrelation lengths depend on the mean height $\bar{h}$ of the atmospheric layer where they are calculated. This is intended to convey the notion that identical separation distances may systematically give rise to diverse overlap behavior in different vertical segments of the atmosphere with distinct cloud formation processes and dynamical characteristics.

ACPD
11, 597–625, 2011

One of the drawbacks of inverse exponential modeling is that negative values of the overlap parameters cannot be captured (Norris et al., 2008). This turns out to be a poorer approximation for the condensate rank correlation, for which negative values are encountered much more frequently than alpha. In the analysis that follows, overlap is discussed both in terms of the overlap parameters alpha and rank correlation and in terms of their respective decorrelation lengths. The latter tend to be more convenient because they provide a simple scalar representation of overlap, while alpha and rank correlation are arrays that encompass the potentially complex full dependence on layer height pairs (z_1,z_2).

3 Overlap characteristics at the SGP ACRF site

3.1 Seasonal cycle of overlap parameters and their decorrelation lengths

To derive the monthly profiles of $\alpha(\Delta z)$ and $r(\Delta z)$ we ensemble-average for each month all values of $\alpha(z_1,z_2)$ and $r(z_1,z_2)$ that have the same separation distance Δz. The number of values that enter this ensemble average decreases monotonically with separation distance. For the time being, we do not distinguish between Δz's at different levels of the atmosphere, although we will examine this dependence later. The monthly values can be further averaged to seasonal averages for winter (DJF), spring (MAM), summer (JJA) and fall (SON). Figure 1 shows seasonal averages of alpha and Fig. 2 shows seasonal averages of rank correlation; the profiles of standard deviation for both quantities are also provided in separate plots. The figures show both the seasonal dependence for a given segment size (150 km) and the dependence on segment size for a given season (JJA was chosen – the dependence is similar for other seasons). As explained above, the three segments sizes, 75, 150, 300 km, should not be taken literally as actual segment spatial scales, but to be roughly corresponding to a fixed number of 720, 1440, and 2880 condensate profiles.

ACPD
11, 597–625, 2011

L. Oreopoulos and P. M. Norris

In the analysis that follows, we will focus mainly on a description of the characteristics of overlap as extracted from the dataset and will not consistently attempt to provide an interpretation of the underlying reasons behind the overlap features that emerge. Such interpretations are often not obvious and would require extensive additional meteorological data not provided by the MICROBASE dataset. A comparison of Figs. 1 and 2 indicates that alpha profiles vary more with season and domain size than rank correlation profiles. They also drop much more slowly with distance compared to rank correlations. The decrease of alpha with separation distance is faster for winter, followed by fall, spring and summer. In other words, cloud fraction overlap is most random in the winter and least random (most maximum) during the summer. Since convective activity is greatest during the summer while winter cloudiness is dominated by frontal systems, the conclusion is that convective clouds are more maximally overlapped than frontal clouds. This was also found by Mace and Benson-Troth (2002) and Naud et al. (2008). The first of these papers actually showed the seasonal cycle of alpha at select separation distances over the same observation site and from a data set derived indepedently from the same suite of instruments used in MICROBASE, but of coarser temporal and vertical resolution.

Our results also indicate that the variability (standard deviation) of alpha profiles follows in general the order of degree of random overlap: the alpha profile with the smallest values (DJF) is also the most variable; during summer the alpha values are larger (more maximally overlapped) and the distribution of alpha values is more narrow. This seems reasonable – if random overlap is produced by independent clouds layers at various heights, then we expect to get many cases of chance alignments between layers on a per segment basis, thereby injecting a random element of "maximum overlap" and increasing the variance of alpha. In contrast, maximum overlap cases produced by convective systems with strong vertical coherence are not expected to produce random overlap by chance, unless there is a strong vertical wind shear.

The choice of domain size affects the alpha profiles significantly. Cloud fraction overlap is more maximum for the largest domain size (300 km). This has been previously

ACPD
11, 597–625, 2011

noted by Hogan and Illingworth (2000) and Oreopoulos and Khairoutdinov (2003) and is the natural outcome of the dominant scales of cloud formation as determined by the underlying dynamical and thermodynamical processes. Indeed, for isolated cloud systems the chance of finding large total cloud fractions decreases as the domain size increases, and since random overlap is associated with larger cloud fractions than maximum overlap for the same cloud fraction profile, the overlap will tend to be more random within a smaller domain. Another thought experiment that leads to the same conclusion – that the overlap is more maximum for a larger domain – is to consider a particular cloud fraction profile within a certain domain. By enlarging the domain without changing the cloud whose spatial extent was determined by the dominant scales of the underlying dynamics and thermodynamics, both the layer cloud fraction and the total cloud fraction decrease (layer clear fractions and total clear fraction increase). The cloud system occupies a relatively smaller portion of the bigger domain and cloud layers appear more aligned (more maximaly overlapped) in the vertical since the combined clear fraction of any two layers has increased.

This type of argument does not carry over trivially to rank correlations which seem to also show the same dependence, albeit weaker, on domain size. At larger domain sizes the probability density function of condensate must in general become wider and the relative ordering of condensate values must change so that the values of particular portions of the domain with more similar clouds are closer in relative strength compared to the case where the domain is smaller and the inter-layer variability in those portions appears larger. In other words, by extending the domain and widening the distribution with the addition of different clouds, the values of condensate at close horizontal positions appear more similar in a relative sense than in the initial (narrower) distributions.

The seasonal ordering in terms of the magnitude of rank correlation profiles is the same as for alpha profiles for separation distances up to ∼4 km where positive values occur. Rank correlations are generally smaller for DJF and progressively increase for MAM and JJA before dropping again for SON. This is consistent with stronger vertical

Discussion Paper | Discussion Paper | Discussion Paper | Discussion Paper |
ACPD
11, 597–625, 2011
An analysis of cloud overlap
L. Oreopoulos and P. M. Norris

motions during the summer producing more aligned columns of cloud condensate. However, the picture reverses for the negative rank correlations of larger separation distances which are greater in absolute value for JJA and smaller (closer to zero) for DJF. Apparently the low and high clouds of summer multi-layer cloud systems are more anticorrelated than in the winter. Since the negative values of alpha do not exhibit such reversal, i.e., DJF cloud fractions are more minimally overlapped than JJA, the conclusion is that for the smaller overlapped portion of DJF clouds the anticorrelations of relative condensate strengths are somewhat weaker. As we will see in the next section, however, when all separation distances and seasons are ensemble-averaged there is a clear tendency for smaller alphas to be correlated with smaller rank correlations. This is not surprising since this is the tendency that Figs. 1 and 2 imply at smaller separations, which are derived from a much larger number of data points. It should also be kept in mind that the dataset used for Figs. 1 and 2 is not identical since overcast layers are excluded from the calculation of alpha but not of rank correlation.

Another difference in the behavior of rank correlations is that the variability of rank correlations is smallest in DJF and greatest in JJA, i.e., the opposite of what takes place for alphas. This is somewhat expected given that the mean profile of rank correlation, itself coming from a wide distribution of segment-length rank correlations, is more extreme in an absolute sense for JJA (more positive at smaller separations, more negative at larger seperations) than DJF. The variability stabilizes to near-constant values at or above smaller separation distances, ∼2 km or below depending on the season, compared to alpha variability which becomes more stable (apart from the superimposed noise of the smaller sample size) only at separation distances above ∼3 km. In conclusion, for both alpha and rank correlations, the variability increases rapidly up to a certain separation distance and then changes more slowly. Also, the standard deviation that the parameters settle to is much larger (0.8–1) for alpha, compared with the rank correlation (0.35–4).

The ensemble-averaged alpha and rank correlation profiles of individual months (not shown) can be fit to inverse exponentials via least squares, following chapter 15.2 of

Press et al. (1992), in order to infer the decorrelation lengths of Eq. (4). The fitting gives greater weight to smaller separation distances which are more numerous. The results for the different segment lengths are given in Fig. 3, as a function of the month of the year. The figure reflects some of the seasonal and spatial scale dependencies discussed previously, for example decorrelation lengths that peak during the summer months when vertical stability is expected to be weaker, and stronger vertical motions favor the formation of cloud systems where cloud fractions and condensates align better. Alpha decorrelation lengths are larger than their rank correlation counterparts, with a stronger seasonal cycle and more pronounced dependence on domain size, echoing the contrasts we highlighted in our discussion of Figs. 1 and 2.

We also calculated, but do not show here, the median values of the decorrelation length derived for each segment and each month, as in Barker (2008b). The profiles of the overlap parameters for each individual segment are much more noisy and the fits much less reliable. Decorrelation lengths of alpha for individual segments can be very large, as also noted by Barker (2008a) (they exceed 10 km 36.5% of the time), making the mean values of limited use, and skewing the medians to values much higher (about double) than those calculated from ensemble-averaged overlap parameter profiles. For the rank correlation decorrelation lengths of individual segments, however, large magnitudes are much rarer (they exceed 10 km only for ~1% of the cases) and the range of values is much narrower. The histograms of the two decorrelation length distributions for all 150 km segments of all months, but without the values greater than 10 km, are compared in Fig. 4. The L_α histogram is much wider, has no well-defined peak and looks quite different from the L_r histogram which peaks at the 0.2–0.4 km bin. Despite the fact that the mode of the latter histogram is very small, the mean derived from the histogram, 1.74 km, is larger than any of the values shown in Fig. 3, which serves as a reminder that the mean of decorrelation lengths derived from individual segments is a fundamentally distinct quantity from the decorrelation length derived from a mean profile of rank correlations. This is even more true for alpha decorrelation length which has an even wider distribution in Fig. 4.

3.2 Dependence of overlap parameters on vertical location

In our earlier discussion of Eq. (4) we mentioned that identical separation distances may give rise to systematically different overlap parameter values in different vertical segments of the atmosphere due to distinct cloud formation processes and associated dynamical circulations. In this subsection we examine whether this can indeed be shown with the available data set. Figure 5 shows ensemble-averaged alphas and rank correlations at separation distances of 1 and 2 km aggregated separately for four different atmospheric layers. The error in the mean is too small to be discernible in these plots and is not shown, but ensures that any differences among the means is always much larger than the standard errors. For alpha, there is a general trend of more random overlap for the same separation distance the higher the atmospheric layer in which the calculation performed. This is always true for the 2 km separation distance, but does not hold true for the 1 km separation distance as one moves from the 0–3 km layer to the 3–6 km layer. The rank correlation behavior, on the other hand, is somewhat less simple. The 0–3 km layer has the largest values at both separation distances, while the smallest are encountered in the 3–6 km layer for the 2 km separation distance and the 9–12 km layer for the 1 km separation distance. The large decrease of the rank correlation from the 0–3 km to the 3–6 km layer can probably be traced back to the cloud phase transition likely to occur within the latter layer and the transition from the dynamic and thermodynamic states of the planetary boundary layer, which tends to be more well-mixed, to those of the free troposphere, which tends to be more dominated by stability. The probability of these transitions actually occurring is greater for 2 km separation distances, which may be the reason for the observed minimum in rank correlation. Hogan and Illingworth (2003) examined the linear correlations of ice water content for overcast clouds above and below 6.9 km. They found greater correlations in the upper layer, a result qualitatively similar to our increase of rank correlation from the 3–6 km layer to the 6–9 km layer, which they attributed to the reduced wind shear of the upper layer. The datasets and methodology are different enough to prevent us

Discussion Paper | Discussion Paper | Discussion Paper | Discussion Paper |

ACPD

11, 597–625, 2011

An analysis of cloud overlap

L. Oreopoulos and P. M. Norris

from drawing definitive conclusions about the apparent consistency of the two findings, but the qualitative agreement is worth mentioning nonetheless. Naud et al. (2008) also studied the role of wind shear on cloud overlap but for cloud fraction only, i.e., the effect on alphas, not rank correlations. They found higher wind shear correlating with smaller alphas above ~2 km separation distances. If shear was the sole dynamical factor regulating cloud overlap then our results would seem to imply that shear must increase with height since according to Fig. 5 cloud fraction overlap tends to be generally more random in the upper troposphere compared to the lower troposphere. In our case, such an interpretation can not be provided with certainty based on the information available here.

3.3 Relationship between overlap parameters

If the overlap parameters alpha and rank correlation are to be used to generate columns of condensate that follow the overlap behavior seen in observations, it may not be wise to choose values for these parameters that are independent of each other. In a modeling application, the most convenient approach would be to deal with scalar quantities such as decorrelation lengths and therefore stay within the framework of exponentially decaying alphas and rank correlations while accepting the shortcoming of positive-only values. A plot like Fig. 3 can be employed to pick L_α and L_r values that can then be used at all times for each month at the appropriate latitudes and domain sizes. This plot implies that the ratio of L_α to L_r changes substantially from month to month (from a minimum of ~2 in February to a maximum of ~2.8 in July and September). The wisdom of picking a single value of L_α and (independently or not) of L_r and applying it universally for a particular month will probably depend on the application and should be the subject of further investigation, as will be discussed in the next section.

If one wants to explore relationships between the two types of overlap, it may not however be appropriate to compare only quantities derived after a large amount of ensemble averaging has been performed, which was the approach we adopted for obtaining meaningful values of decorrelation lengths. We will therefore return to

ACPD
11, 597–625, 2011

segment-level alphas and rank correlations for our investigation of the relationship between cloud fraction and condensate distribution overlap. We will also investigate whether rank correlations depend on the combined cloud fraction of two layers. The latter is not independent of alpha since for a given pair of cloud fractions, a smaller alpha implies a larger combined cloud fraction. So, while we may get a somewhat different perspective by looking at how ranks change with different combined cloud fractions, that perspective cannot be inconsistent from the one obtained by looking at rank correlation vs. alpha relationships.

In order to examine these relationships both overlap parameters need to be derived from the same data set. Since alpha is meaningless when one of the two layers is overcast while a rank correlation is not, for the purposes of this subsection we infer both overlap parameters only when the overlapped portion of the two layers has at least 0.01 cloud fraction (to have enough data points for an acceptable rank correlation calculation) and when neither of the two layers has a cloud fraction greater than 0.99. We create two types of plots: one showing the frequency distribution of rank correlations for different bins of combined true cloud fraction or alpha, and one showing the ensemble mean ranks and fraction of negative mean ranks for those bins. The second type of plot essentially summarizes two features, the mean and the cumulative frequency up to zero rank correlation, found in the plots of the first type, but for more bins than were convenient to display in those plots.

The plots discussed above are shown in Figs. 6 and 7. Figure 6 suggests that when the combined cloud fraction of the layers is 1 the probability distribution of rank correlations is almost perfectly symmetric around zero and yields a near-zero mean rank. This is an interesting result that defies an obvious explanation. Combined cloud fractions of exactly 1 can occur only for overlap smaller than random, i.e., for some degree of minimum overlap. So it would be tempting to infer that so-called minimal overlap, which implies a smaller overlapped fraction, tends to be associated with zero mean rank correlation, but with a large amount of noise of either signed rank due to the small overlapped sample size.

However, there are significant and hitherto undiscussed interpretation issues that may be appropriate to raise here. Up until this point we have been treating alpha and rank correlation on somewhat of an equal footing. In fact, however, they are quite different – rank correlation is a fairly robust statistical property based on a typically large number of rank pairs in the overlapped portion of the two layers. Alpha, by contrast, for a particular layer pair is based on only the two layer cloud fractions, and is not a statistically robust quantity unless averaged over an ensemble of many segments or unless the single segment in which it is evaluated is large compared to the horizontal length scale l_h over which individual clouds in each layer become statistically uncorrelated. In other words, while single segment $\alpha(z_1, z_2)$ values of 1, 0 and <0 do have specific meanings for the segment in terms of cloud overlap (maximum, random and some degree of minimum overlap) they imply little about the respective large-scale statistical overlap of the two cloud layers over a large number of segments, unless the segment is large enough to contain many dynamically independent cloud samples. This is presumably why the standard deviations of alpha in Fig. 1 are so much larger and more variable than the respective rank correlation values of Fig. 2.

Now, let us apply this thinking to the example of 100% combined cloud fraction being discussed above. Such a case implies $\alpha(z_1, z_2)<0$ (some degree of minimal overlap), however, two completely uncorrelated cloud layers (in the large-scale sense) can frequently produce cases of 100% combined cloud cover in segments that are not large compared to l_h. In fact, the greater the individual layer cloud fractions, the greater the likelihood of this. Thus the 100% combined cloud fraction bin will be a "degenerate bin" that mixes many segments of large-scale uncorrelated layers with perhaps occasional segments of large-scale minimally overlapped layers. If these uncorrelated cases dominate, as they appear to, then it is not surprising that the condensate rank correlations within the bin are near zero in the mean. In this case, "minimal overlap" is likely to be a false designation, since the alphas are all single segment values.

Discussion Paper | Discussion Paper | Discussion Paper | Discussion Paper |

ACPD

11, 597–625, 2011

An analysis of cloud overlap

L. Oreopoulos and P. M. Norris

Title Page
Abstract Introduction
Conclusions References
Tables Figures
◀◀ ▶▶
◀ ▶
Back Close
Full Screen / Esc
Printer-friendly Version
Interactive Discussion

Returning to Fig. 6, a progressive shift to fewer negative and greater mean rank correlations occurs when the combined cloud fractions become smaller, i.e., when the overlap becomes closer to maximum and the individual cloud fractions are also small. One possible explanation is a transition from large scale cloudiness (with large cloud fractions in either or both layers, yielding a large combined fraction, but from layers that can be quite unrelated) to convective clouds (typically small cloud fractions, but a large vertical extent). Note that the 0.9–0.99 combined cloud fraction bin is quite distinct from the overcast case in terms of the rank correlations it contains. Within this bin, random cloud fraction overlap is possible, and positive ranks occur about 62% of the time. By the time the combined cloud fraction is between 0.01 and 0.1 about 80% of the rank correlations are positive.

Figure 7 is consistent with the above picture, since as it was explained earlier, the combined cloud fraction and alpha are not independent. For negative alpha the distribution of rank correlations is again almost perfectly symmetric around zero, and results in an almost exact zero mean rank correlation. As cloud fraction overlap transitions from random to maximum the distributions become progressively more negatively skewed and produce higher mean ranks until exact maximum overlap (alpha=1) is reached. For that bin the number of negative rank correlations goes up again and the value of the mean goes down, making it very distinct from the 0.9–0.99 alpha bin (near-maximum overlap) which contains the largest mean rank, larger even than any mean rank appearing in Fig. 6. Bear in mind that Eq. (1) indicates that the alpha=1 bin does not necessarily contain only small combined cloud fractions, so it should not be associated with any particular true combined cloud fraction bin in Fig. 6. A large value of alpha simply suggests that the probability of a small combined cloud fraction is statistically high.

ACPD
11, 597–625, 2011

4 Discussion of modeling implications

We have presented an analysis of cloud overlap behavior at a mid-latitude observational facility based on retrievals of cloud condensate from a millimeter cloud radar assisted by a suite of other ground instruments. The temporal (horizontal in an eulerian sense) and vertical resolution of the data, at 10 s and 45 m, respectively, are the highest ever used to study this problem. The two facets of overlap that were investigated were cloud fraction overlap (previously examined at the same site with coarser resolution datasets by Mace and Benson-Troth, 2002 and Naud et al., 2008) and the overlap of horizontal distributions of condendsate, which has never been previously examined with a dataset of this type. Besides the cloud fraction overlap parameter alpha and the rank correlation coefficient, the degree of proximity to the random and maximum overlap assumptions was also expressed in terms of decorrelation lengths, a convenient scalar parameter that emerges under the approximation of overlap parameters decaying exponentially with separation distance. Our findings regarding cloud fraction overlap, whether expressed in terms of alpha or its decorrelation length, reaffirm previous results with respect to seasonal variations and dependence on domain size, namely that overlap tends to be more maximum for summer months and larger domains. The same dependence is found for rank correlation, albeit significantly weaker, a behaviour that was not previously known. We sought to gain further insight into overlap parameter dependencies by examining differences in mean values for fixed separation distances within different layers of the atmospheric column, and by searching for possible systematic relationships between alpha and rank correlation. These efforts revealed that for the same separation distance the overlap parameters are significantly different at the various atmospheric layers, and that random cloud fraction overlap tendencies are generally in sync with more random distributions of relative condensate strength.

The question that naturally arises is whether any of the above has practical implications. If one wants to create 2-D X-Z distributions of condensate (a second horizontal dimension is irrelevant for fields with no predefined spatial coherence) starting from

ACPD
11, 597–625, 2011

profiles of cloud fraction and the mean and variance of cloud condensate, overlap rules must be established. Our paper contains essential information about these overlap rules. Obviously, an extension to a global dataset is desirable, and the combined CloudSat/CALIPSO (Stephens et al., 2002) dataset may be of significant help in this regard. Also, a measure of whether overlap has been successfully and realistically implemented is necessary. A straightforward avenue of future research is to adopt the inverse exponential model and express overlap in terms of decorrelation lengths. Our dataset has shown that negative values for the overlap parameters are too frequent for the exponential framework to be consistently credible, but whether it still works sufficiently well with all negative values set to zero remains a legitimate subject of further investigation. Then there is the question what value of decorrelation length to use. Should the median of individual decorrelation lengths (derived from individual data segments) be used as in Barker (2008b)? Apply also a modified definition that yields an "effective" decorrelation length where the additional constraint of matching segment-level total cloud fractions is imposed (Barker 2008b)? Or use the decorrelation length as derived in this work, namely from fits to ensemble-averaged profiles of alpha and rank correlation?

A research path may be available to help address these questions (e.g., see Barker 2008a, b). It essentially entails using the profiles of cloud fraction and the first two moments of condensate for each data segment, assuming a probability distribution function for the condensate, and reconstructing the cloud fields using either a single decorrelation length from average overlap parameter profiles or individual decorrelation lengths derived at the segment level, with a cloud generator of the type introduced by Räisänen et al. (2004). The appropriateness of the inverse-exponential model and of the proper decorrelation lengths can be tested by comparing: (a) cloud statistics (total cloud fraction or cumulative profiles of cloud fraction exposed to space and moments of water path) between the original and reconstructed cloud fields and (b) radiation flux and heating rates corresponding to the original and reconstructed cloud fields. Radiative comparisons of the latter type will be facilitated in the near future by the recent

ACPD
11, 597–625, 2011

release of the Radiatively Important Properties Best Estimate (RIPBE) evaluation product (MacFarlane, personal communication, 2010) for the SGP ACRF site. RIPBE relies for its cloud specification on the same MICROBASE dataset we use for our overlap analysis (albeit at a lower 1 min temporal resolution), while also including all other atmospheric (temperature and water vapor profiles, aerosol loading, etc.) and surface (spectral albedo) variables that are required for full broadband radiative transfer calculations. Such a dual evaluation is in our future plans.

Acknowledgement. The authors gratefully acknowledge support by the US Department of Energy, Office of Science, Office of Biological and Environmental Research, Environmental Sciences Division as part of the ARM program under grant DE-FG02-07ER64354, and by the NASA Modeling Analysis and Prediction and CloudSat/CALIPSO Science Team Recompete programs managed by David Considine. We would like to thank Mike Jensen and Maureen Dunn of Brookhaven National Lab for generating and providing the MICROBASE data that served as the backbone of our analysis.

References

Barker, H. W., Stephens, G. L., and Fu, Q.: The sensitivity of domain-averaged solar fluxes to assumptions about cloud geometry, Q. J. Roy. Meteor. Soc., 125, 2127–2152, 1999.

Barker, H. W.: Overlap of fractional cloud for radiation calculations in GCMs: a global analysis using CloudSat and CALIPSO data, J. Geophys. Res., 113, D00A01, doi:10.1029/2007JD009677, 2008a.

Barker, H. W.: Representing cloud overlap with an effective decorrelation length: an assessment using CloudSat and CALIPSO data, J. Geophys. Res., 113, D24205, doi:10.1029/2008JD010391, 2008b.

Clothiaux, E. E., Ackermann, T. P., Mace, G. C., Moran, K. P., Marchand, R. T., Miller, M. A., and Martner, B. E.: Objective determination of cloud heights and radar reflectivities using a combination of active remote sensors at the ARM CART sites, J. Appl. Meteor., 39, 645–665, 2000.

Hogan, R. J. and Illingworth, A. J.: Deriving cloud overlap statistics from radar, Q. J. Roy. Meteor. Soc., 126, 2903–2909, 2000.

Hogan, R. J. and Illingworth, A. J.: Parameterizing ice cloud inhomogeneity and the overlap of inhomogeneities using cloud radar data, J. Atmos. Sci., 60, 756–767, 2003.
Liao, L. and Sassen, K.: Investigation of relationships between Ka-band radar reflectivity and ice and water content, Atmos. Res., 34, 231–248, 1994.
Liu, C. L. and Illingworth, A.: Toward more accurate retrievals of ice water content from radar measurements of clouds, J. Appl. Meteor., 39, 1130–1146, 2000.
Mace, G. G. and Benson-Troth, S.: Cloud layer overlap characteristics derived from long-term cloud radar data, J. Climate, 15, 2505–2515, 2002.
Miller, M. A., Johnson, K. L., Troyan, D. T., Clothiaux, E. E., Mlawer, E. J., Mace, G. G.: ARM Value-Added Cloud Products: Description and Status, in: Proceedings of the 13th ARM Science Team Meeting, US Department of Energy, Washington, DC, available at http://www.arm.gov/publications/proceedings/conf13/extended_abs/miller-ma.pdf, 2003.
Naud, C. M., Del Genio, A., Mace, G. G., Benson, S., Clothiaux, E. E., and Kollias, P.: Impact of dynamics and atmospheric state on cloud vertical overlap, J. Climate, 21, 1758–1770, doi:10.1175/2007JCLI1828.1, 2008.
Norris, P. M., Oreopoulos, L., Hou, A. Y., Tao, W. K., and Zeng, X.: Representation of 3-D heterogeneous cloud fields using copulas: theory for water clouds, Q. J. Roy. Meteorol. Soc., 134, 1843–1864, 2008.
Oreopoulos, L. and Khairoutdinov, M.: Overlap properties of clouds generated by a cloud-resolving model, J. Geophys. Res., 108(D15), 4479, doi: 10.1029/2002JD003329, 2003.
Press, W. H., Teukolsky, S. A., Vetterling, W. T., and Flannery, B. P.: Numerical Recipes in Fortran 77, the Art of Scientific Computing, 2nd ed., Cambridge University Press, Cambridge, 933 pp., 1992.
Pincus, R., Barker, H. W., and Morcrette, J. J.: A fast, flexible, approximate technique for computing radiative transfer in inhomogeneous cloud fields, J. Geophys. Res., 108(D13), 4376, doi:10.1029/2002JD003322, 2003.
Pincus, R., Hannay, C., Klein, S. A., Xu, K.-M., and Hemler, R.: Overlap assumptions for assumed probability distribution function cloud schemes in large-scale models, J. Geophys. Res., 110, D15S09, doi:10.1029/2004jd005100, 2005.
Räisänen, P., Barker, H. W., Khairoutdinov, M., Li, J., and Randall, D. A.: Stochastic generation of subgrid-scale cloudy columns for large-scale models, Q. J. Roy. Meteor. Soc., 130, 2047–2067, 2004.
Shonk, J. K. P., Hogan, R. J., Edwards, J. M., and Mace, G. G.: Effect of improving represen-

ACPD
11, 597–625, 2011

An analysis of cloud overlap

L. Oreopoulos and P. M. Norris

tation of horizontal and vertical cloud structure on the Earth's global radiation budget. Part I: Review and parametrization, Q. J. Roy. Meteor. Soc., 136, 1191–1204, doi:10.1002/qj.647, 2010.

Stephens, G. L., Vane, D. G., Boain, R. J., Mace, G. G., Sassen, K., Wang, Z., Illingworth, A. J., O'Connor, E. J., Rossow, W. B., Durden, S. L., Miller, S. D., Austin, R. T., Benedetti, A., Mitrescu, C., and the CloudSat Science Team: The CloudSat mission and the A-Train: a new dimension of space-based observations of clouds and precipitation, Bull. Am. Meteor. Soc., 83, 1771–1790, 2002.

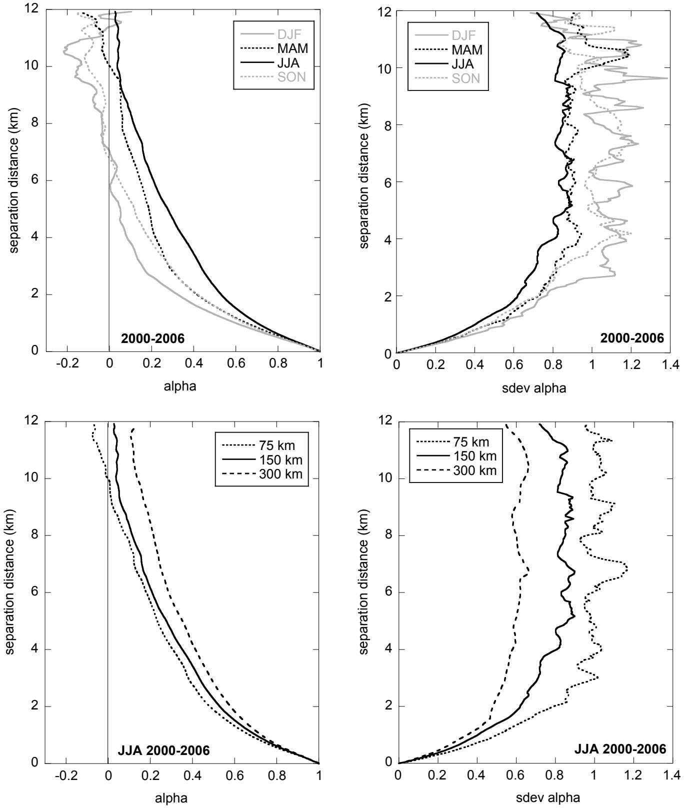

Fig. 1. Profiles of seasonal ensemble means (left panels) and standard deviations (right panels) of the overlap parameter alpha as a function of separation distance calculated from the 7-year Microbase dataset. Top panels are for the 150 km segment size and all four seasons: December-January-February (DJF, winter), March-April-May (MAM, spring), June-July-August (JJA, summer), September-October-November (SON, fall). Bottom panels are for different segment sizes for JJA.

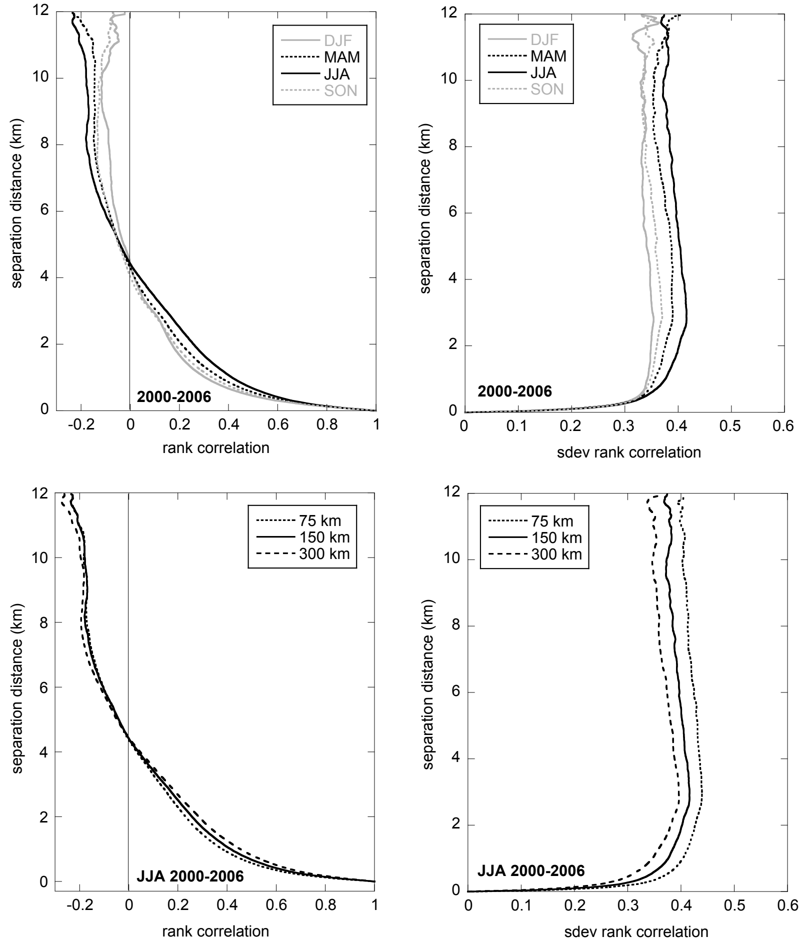

Fig. 2. As in Fig. 1, but for rank correlations.

ACPD
11, 597–625, 2011

An analysis of cloud overlap

L. Oreopoulos and P. M. Norris

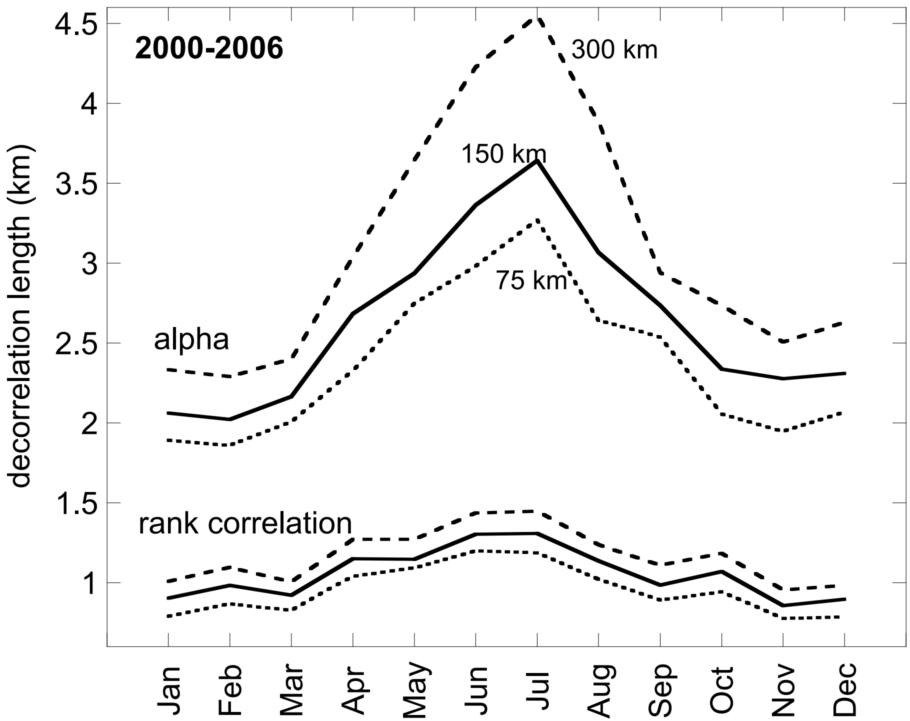

Fig. 3. The seasonal cycle of L_α (top three curves) and L_r (bottom three curves) decorrelation lengths from ensemble-averaged profiles of alpha and rank correlation like those shown in Figs. 1 and 2, but on a monthly instead of tri-monthly scale. The L_r curves are ordered in terms of segment size in the same manner as the L_α curves.

ACPD
11, 597–625, 2011

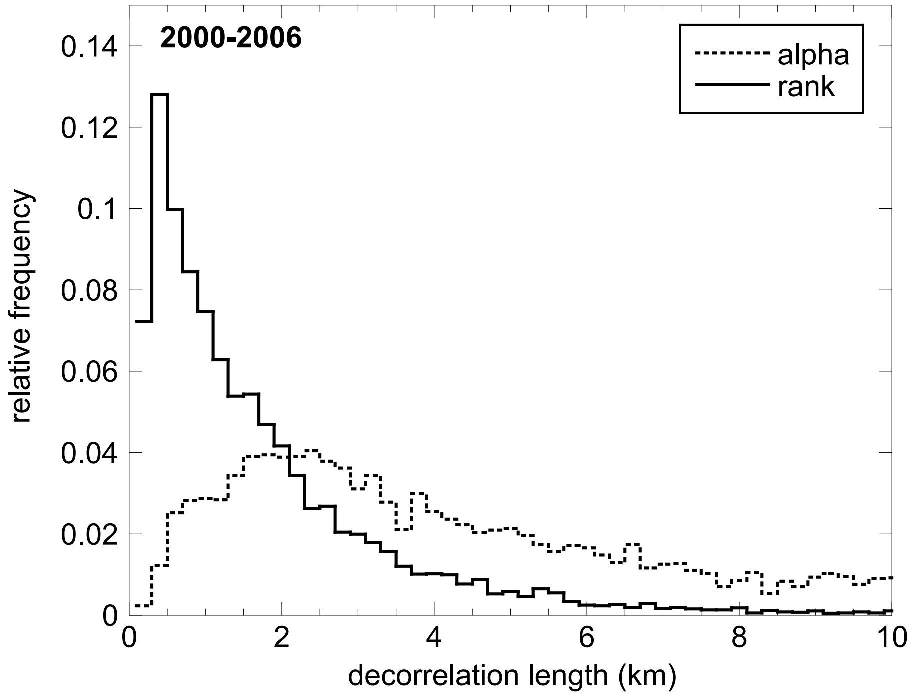

Fig. 4. Histograms of L_α and L_r derived from individual 150 km segments. Due to the existence of a large fraction of L_α values greater than 10 km (indicative of near-maximum overlap conditions), both histograms were renormalized with such values excluded.

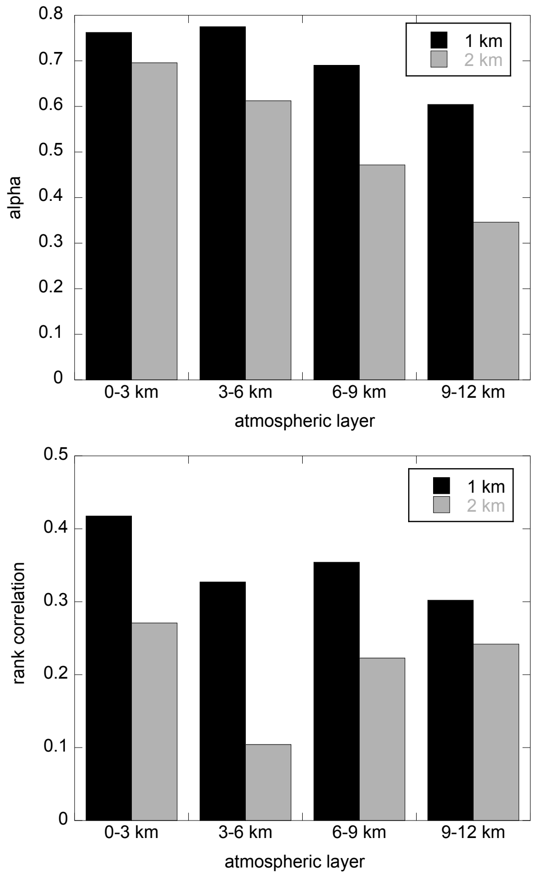

Fig. 5. Alphas (top) and rank correlations (bottom) for the 150 km segment size and separation distances of 1 and 2 km when ensemble-averaged separately within four 3 km thick atmospheric layers. 0–3 km corresponds to the atmospheric layer closest to the surface.

ACPD
11, 597–625, 2011

An analysis of cloud overlap

L. Oreopoulos and P. M. Norris

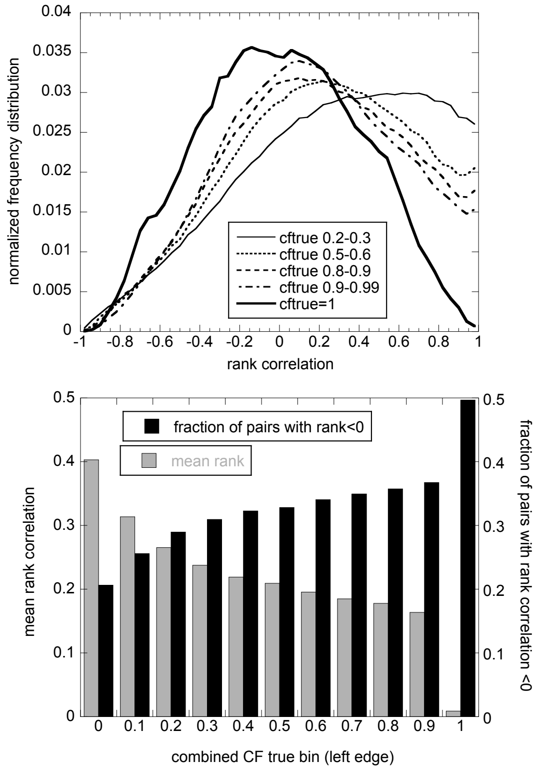

Fig. 6. (Top) histograms of rank correlations for different bins of true combined cloud fraction calculated from layer pairs taken at every possible separation distance within 150 km segment sizes; (bottom) ensemble-averaged rank correlations and fraction of negative rank correlations within true combined cloud fraction bins from the same dataset used for the top panel. The value below each pair of bars in the lower panel is the left edge of the bin. For example 0.1 refers to the interval [0.1,0.2), and the last bin is for a combined cloud fraction exactly equal to one.

ACPD
11, 597–625, 2011

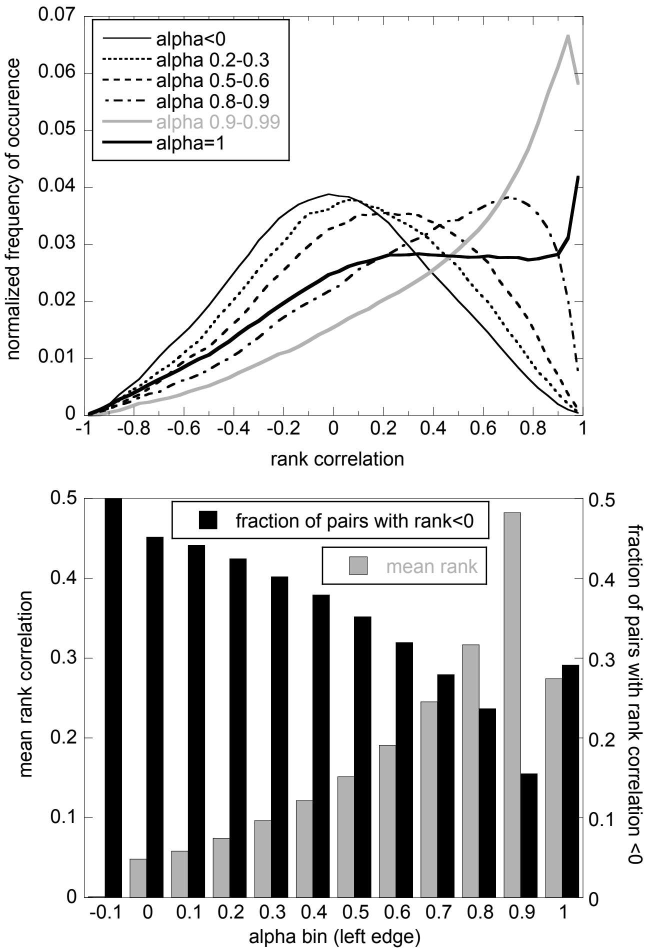

Fig. 7. As in Fig. 6, but for bins of overlap parameter alpha.

ACPD
11, 597–625, 2011